sustainability

MDPI

Article

Influence of Joint Characteristics on Crack Propagation during the Double-Hole High-Energy Gas Impact Permeability Enhancement Process

Dong Duan [1,2,*], Xi Chen [1,2], Xiaojing Feng [1,2], Wenbo Liu [1,2], Hongzhi Zhang [1,2], Xiaoyu Chen [1,2], Shilei Gao [1,2], Xin Wang [1,2] and Ao Wang [1,2]

[1] College of Mining Engineering, Taiyuan University of Technology, Taiyuan 030024, China
[2] Key Laboratory of In-Situ Property-Improving Mining of Ministry of Education, Taiyuan University of Technology, Taiyuan 030024, China
* Correspondence: duandong@tyut.edu.cn; Tel.: +86-15135153856

Abstract: In view of current research on the cracking mechanism of high-energy gas on coal, little attention has been paid to imitating the law of explosive blasting and cracks propagation, and the influence of joint on cracks propagation in the process of high-energy gas impact permeability enhancement has not been taken into account. In this paper, the effects of joint dip angles and joint lengths on cracks size propagation are studied by using a similar simulation test and RFPA2D-dynamic numerical simulation software. In the process of impact permeability enhancement of high-energy gas, the extension direction of the cracks is approximately parallel to the joint, and with the increase in the dip angle and length, the higher the number of cracks, the larger the extension range, and the closer it is to the permeability enhancement holes, the fracture network is formed. When the dip angle of the joint is 30°, the impact permeability enhancement effect results in an obvious zoning phenomenon. When the joint dip angle is 60° and 90°, there is a higher number of cracks and the cracks network is formed, and with the increase in the dip angle, the more the cracks develop and the better the impact permeability enhancement effect.

Keywords: double-hole permeability enhancement; high-energy gas impact permeability enhancement; joint characteristics; quantitative characterization; cracks propagation

Citation: Duan, D.; Chen, X.; Feng, X.; Liu, W.; Zhang, H.; Chen, X.; Gao, S.; Wang, X.; Wang, A. Influence of Joint Characteristics on Crack Propagation during the Double-Hole High-Energy Gas Impact Permeability Enhancement Process. *Sustainability* **2022**, *14*, 16342. https://doi.org/10.3390/su142416342

Academic Editors: Danqi Li, Ping Chang, Saisai Wu and Jianhang Chen

Received: 1 November 2022
Accepted: 4 December 2022
Published: 7 December 2022

1. Introduction

As a kind of unconventional natural gas, gas is not only a valuable clean energy, but also a high-quality fuel. The calorific value of 1 m^3 pure coal-bed methane is equivalent to 1.13 kg gasoline or 1.21 kg standard coal. The direct emission of gas not only aggravates the atmospheric greenhouse effect and environmental pollution, but also is a great waste of energy resources. Therefore, the extraction of gas can not only effectively reduce the mine gas concentration to avoid gas explosion, but also play an important role in slowing down the greenhouse effect and providing clean alternative energy. So, mining coal-bed methane is in line with China's dual carbon strategic decision. Under this background, domestic and foreign scholars have put forward a variety of local pressure relief and permeability enhancement methods for high gas and low permeability coal seams, including hydraulic fracturing technology, hydraulic slotting technology, hydraulic punching technology, blasting technology and CO_2 phase change technology, etc. [1–14]. Compared with the above methods, the high-energy gas impact permeability enhancement technology not only fully takes into account their advantages, but also abandons their disadvantages; that is, no secondary pollution of coal seam, no sparks, controllable gas pressure, repeatable impact and so on. It is a promising technology for increasing permeability in a single low permeability coal reservoir [15–17].

In the aspect of impact permeability enhancement of double-hole blasting, Guo D.Y. [18,19] pointed out that the superposition effect of a stress wave between two blasting holes can restrain the expansion of cracks in some regions. Fan S.X. et al. [20] designed two fracturing holes using the L-CO_2 fracturing test and proved that the fracturing radius of the fracturing holes was about 25 m under pressure 30 MPa. Song Y.Q. et al. [21] used ANSYS to build a three-dimensional porous blasting model in the same section, which improved the gas extraction rate. In the field fracturing test and laboratory research, scholars have studied the impact stress wave shape of high-energy gas impact permeability enhancement in different ways. For example, Mingxiaotian et al. [22] used MATLAB software to simulate and analyze downhole high-energy gas fracturing. Chen Huabin et al. [23] carried out on-site oil and gas well potential tapping in Tarim Oilfield. Ma Tiehua et al. [24] established an information acquisition platform for studying the performance and mechanism of high-energy gas fracturing in coalbed gas wells. In the experimental process, it is found that the waveform of pressure changing with time is a triangular wave. Therefore, in this paper, the use of a triangular wave as the input waveform is in line with the actual situation.

As the product of a variety of polymer biochemical processes and geological sedimentation, coal usually contains joints of different scales, and these discontinuity structures have a significant impact on its failure behavior under external loads. Li H.W. et al. [25] carried out cyclic cold loading on coal samples and concluded that the joint structure damage of coal samples with a 45° dip angle was the most obvious, and the damaging effect of 60° was the weakest. Mou H.W. et al. [26] carried out uniaxial compression tests on coal samples with different loading directions and joint dip angles, and found that the peak load and failure time decreased at first and then increased with the increase in the angles. Zhao J. J. et al. [27] concluded that the cracks in coal tended to propagate along the joint and the failure area of the joint in the coal body decreased with the increase in crustal stress.

To sum up, the existence of joint in coal makes the permeability enhancement mechanism of high-energy gas impact more complicated. When the external load stress wave propagates to the discontinuity structure the wave propagation will change. This change may strengthen or weaken the failure effect. On the one hand, the existence of the discontinuous surface will hinder the propagation of the stress wave, and its energy attenuates greatly at the surface, which weakens the damage degree of the stress wave propagation direction. on the other hand, when the stress wave propagates to the discontinuous structure, it will be reflected, the stress wave increases, and the damage is serious. Therefore, the study of the influence of joint characteristics on the impact permeability enhancement of high-energy gas can provide a basis for the selection of reasonable parameters and schemes in engineering practice, and has important theoretical and engineering significance.

2. Materials and Methods

2.1. Similar Experimental Research on High-Energy Gas Impact Permeability Enhancement

2.1.1. Test Equipment and Test description

In this study, the similar experiment of high-energy gas impact permeability enhancement is carried out by using the self-made air pressurization system, and a set of experimental equipment for simulating high-energy gas impact cracking is designed and established independently, as shown in Figure 1. The relevant test equipment is shown in Figure 2. The device comprises a control system, a pressurization system and a connecting system. The control system is composed of a pressure gauge and a manual control valve, and the system shows the current gas pressure through the pressure gauge. The pressurization system of the device is composed of an air source and a high-pressure air pump, and its function is to increase the energy by compressing the air. When the high-energy gas reaches the specified pressure value, the high-energy gas is instantly released by manual control of the valve to achieve the purpose of impact. The connecting system is composed of a check valve, a stainless-steel pipe and a connecting valve. The purpose of setting the check valve is to prevent the high-energy gas from reflux and pollute the gas source. The

stainless-steel pipe is not only to ensure the safety of the experimental process, but also to maintain pressure in the experimental process. The purpose of connecting the valve is for the repeatable, quick and convenient connection between the concrete specimen and the system. The concrete specimen is a cement mortar specimen with a particle diameter less than 0.5 mm quartz sand as aggregate, and the sand-binder ratio is 3:1. It is formed by vibrating in the geometric dimension of 150 mm × 150 mm × 150 mm cube specimen mold. At the same time, two standard specimens of 50 mm × 100 mm are poured to measure the physical and mechanical parameters of the sample, as shown in Table 1.

Table 1. Mechanical parameters of specimen.

Sand-Binder Ratio	Unit Weight (kg/m^3)	Compressive Strength (MPa)	Tensile Strength (MPa)	Elastic Modulus (GPa)	Poisson Ration
3:1	2.7	33	2.2	48	0.25

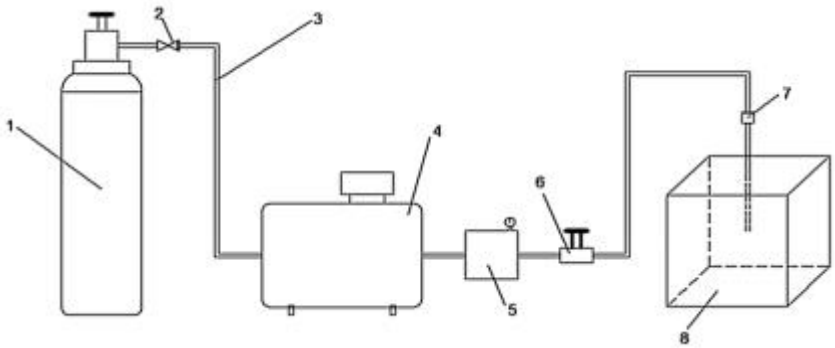

Figure 1. Experimental device for cracking caused by high-energy gas impact permeability enhancement. (1—clean air source; 2—check valve; 3—stainless steel pipe; 4—high pressure air pump; 5—pressure gauge; 6—manual control valve; 7—connection valve; 8—concrete specimen).

(**a**)

(**b**)

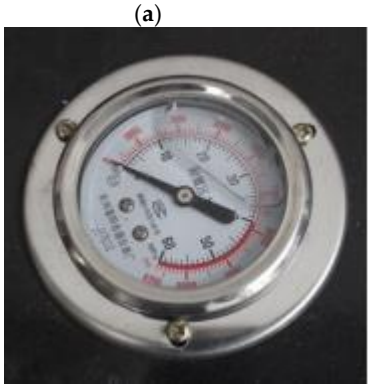

(**c**)

(**d**)

Figure 2. Test equipment: (**a**) connection valves; (**b**) high pressure air pump; (**c**) pressure gauge; (**d**) manual control valve.

Before the start of the test, connect the equipment and build a high-energy gas impact test platform according to the experimental device of high-energy gas impact permeability enhancement in Figure 1. First of all, the specimen is loaded into the clamping device, and a small amount of confining pressure is applied around it, which is used to fix the

concrete specimen and prevent the test piece from spattering during the test. Secondly, the connection valve is assembled, and the pressure pipe of the concrete specimen is connected with the high-energy gas impact test platform. The connected stainless-steel pipe is fixed with a fixture. Thirdly, start the pressurization system of the test device to continuously pressure the clean air source to the pipeline through the booster pump. Finally, after many attempts, it is found that when the pressure gauge is 30 MPa, the concrete specimen can be cracked by opening the manual control valve and instantly releasing high-energy gas and impacting the permeability enhancement hole wall of the concrete specimen.

2.1.2. Strain Gauge Arrangement of Specimen

In order to study the function and propagation law of stress wave in a high-energy gas impact test, a XH5699 dynamic and static resistance strain gauge is used to detect the propagation of stress wave in concrete specimen during cracking. The strain gauge on the surface of the specimen is arranged, as shown in Figure 3. In order to obtain as much data as possible, the strain gauges are fan-shaped around the holes. The strain peak is measured by the statistical strain gauge, the strain peak of the circular holes is taken as the average of the strain peak at the same distance, the peak pressure in Figure 4 is recorded by the strain gauge in this process, and the values of the strain peak in the two directions are compared. It can be seen that the stress wave propagates uniformly in a circle in the specimen. The strain peak at 20 mm is about 40% of 5 mm, and that at 45 mm is 25% and 10% at 70 mm, which shows that the attenuation of a stress wave in the process of propagation has a numerical law.

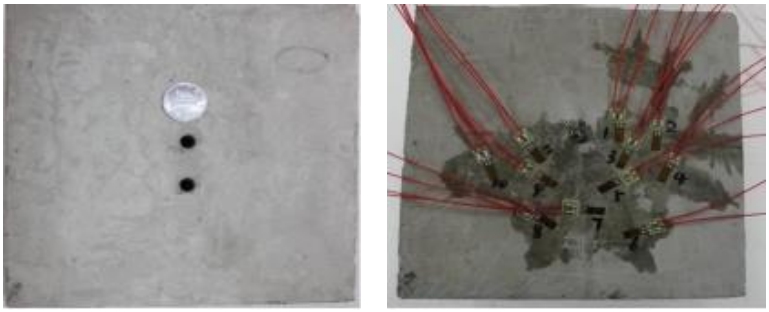

(**a**) (**b**)

Figure 3. Schematic diagram of test specimen and strain gauge layout: (**a**) Test specimen; (**b**) Strain gauge layout diagram.

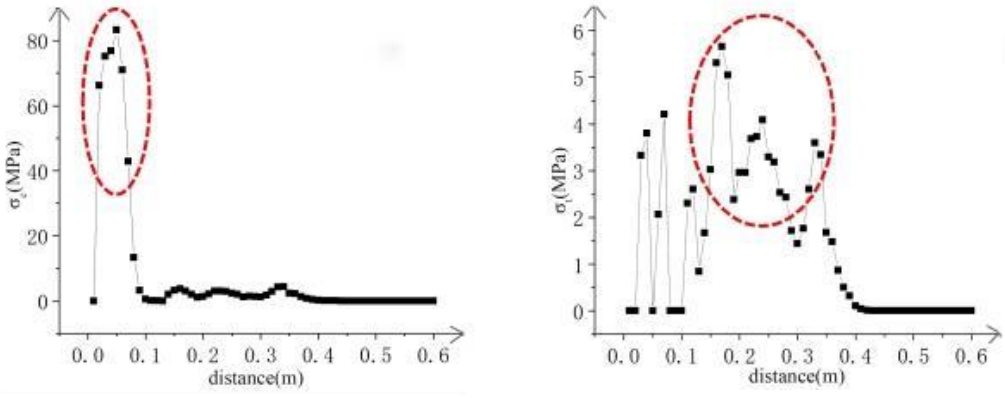

(**a**) (**b**)

Figure 4. Numerical curve of stress on the right side of permeability enhancement holes. (**a**) Radial compressive stress at different distances (The content in the red circle means that the radial compressive stress is greater than the compressive strength). (**b**) Circumferential tensile stress at different distances (The content in the red circle means that the circumferential tensile stress is greater than the tensile strength.).

2.2. Numerical Simulation Research on High-Energy Gas Impact Permeability Enhancement

2.2.1. Introduction of RFPA2D-Dynamic Software

RFPA numerical simulation software is used to study the process from damage to macroscopic fracture of rock. RFPA2d-dynamic is the dynamic analysis version of RFPA, which can be used to carry out numerical experiments on the law of stress wave transmission and induced fracture process of brittle rock materials under dynamic loading. In the dynamic analysis, the software can accept the stress wave as the input and analyze the gradual deformation and fracture process according to the time step under the condition of a given reasonable time step. Thus, the influence of material inhomogeneity on the propagation process of a stress wave and the basic law of the stress wave-induced fracture process can be discussed.

2.2.2. Description of Numerical Simulation Schemes

In this study, the two-factor and three-level orthogonal test method is adopted to design the experimental schemes, as shown in Table 2, the two factors are: joint dip angle and joint length. The three levels of joint dip angle are 30°, 60° and 90°, and the three levels of joint length are 0.2 m, 0.4 m and 0.6 m.

Table 2. Schedules of experiment.

Scheme	1	2	3	4	5	6	7	8	9
Joint dip angle/°	30	30	30	60	60	60	90	90	90
Joint length/m	0.2	0.4	0.6	0.2	0.4	0.6	0.2	0.4	0.6

The research uses RFPA2D-dynamic numerical simulation software; the model size is 1.5 m ×1.5 m and 300 × 300 grids are divided, in which two permeability enhancement holes with 50 mm diameter are excavated with a hole spacing of 0.6 m. There is an open joint between the two holes. The peak value of the impact triangular wave p = 30 MPa is applied, the rise time of the impact triangular wave is $t_1 = 1 \times 10^{-6}$ s, the attenuation time of the impact triangular wave is $t_2 = 5 \times 10^{-6}$ s, and the time step of the impact triangular wave is $\Delta t = 2 \times 10^{-7}$ s, as shown in Figure 5. The joint shape and width of different research schemes are the same: the joint's shape is straight, and the joint's width is 4 cm to reduce the influence on the experimental results.

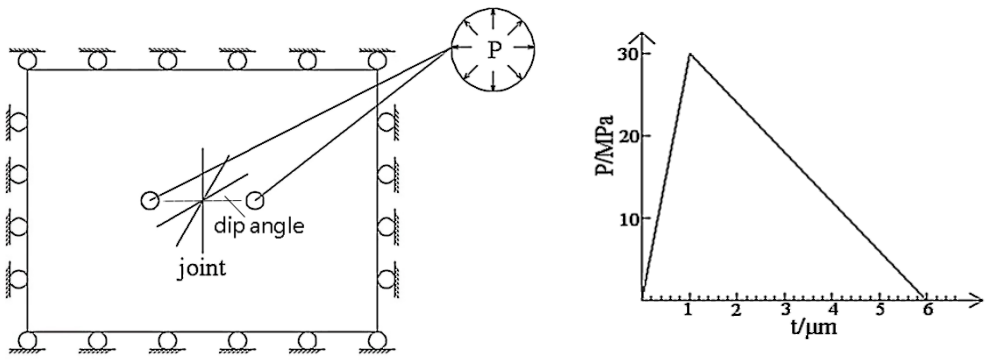

(**a**) (**b**)

Figure 5. Analyze the model geometry and stress curve of applied load: (**a**) Analyze the model geometry (take the joint length of 0.6 m as an example); (**b**) stress curve of applied load.

2.2.3. Evolution of Impact Stress Wave and Division of Failure Zone

In the process of impact permeability enhancement of high-energy gas, the wave gradually attenuates to impact wave, stress wave and seismic wave, forming three different

zones: crushing zone, crack zone and elastic-plastic zone, as shown in Figure 6. Among them, the crushing zone is mainly caused by the impact waves (the radial compressive stress exceeds the compressive strength of the coal), and the crack propagation is mainly caused by the stress waves (the circumferential tensile stress exceeds the tensile strength of the coal). The elastic-plastic zone is mainly formed by seismic waves.

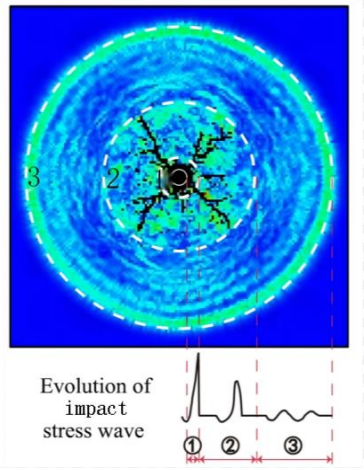

Figure 6. The division of failure zone and the evolution of impact stress wave (1—Crushing zone; 2—Crack zone; 3—Elastic-plastic zone; ①—Impact wave; ②—Stress wave; ③—Seismic wave).

2.2.4. Quantitative Processing of Cracks and Failure Zone

The numerical simulation result image is binarized by using VCTiS for Binary software, and the crack's length and damage zone are measured according to the process of gray transformation, zone statistics, measurement and so on, as shown in Figure 7.

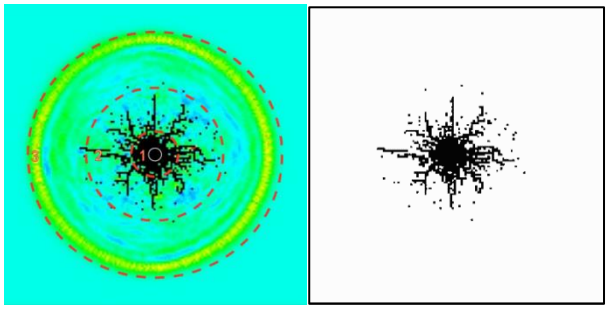

Figure 7. The result of cracks binarization.

3. Results and Discussion

3.1. Influence of Joint Dip Angle on Cracks Propagation Law

Due to the limitation of space, the cracks propagation process is analyzed by taking the joint length of 0.4 m as an example. The RFPA2D-dynamic simulation software completely shows the failure evolution process of coal under the action of impact wave during high-energy gas impact permeability enhancement, and dynamically reproduces the initiation, gestation and forming process of the crushing zone, radial crack zone and elastic-plastic zone around the permeability enhancement holes, as shown in Figure 8.

Under the action of shock wave, the walls of the permeability enhancement holes are broken (Step 20). As the shock wave attenuates to stress wave, four uniform and symmetrical main cracks appear around the wall of each hole, and the length of the main cracks is 40 mm.

With the propagation of a stress wave in coal (step 40), when the joint dip angle is 30°, the length of the six main cracks increases to 80 mm, and the length of the main cracks

close to the joint end is 40 mm, without further extension. This is because the stress wave attenuates and transfers at the joint end, and two cracks with a length of 80 mm appear on the side of the joint end near the holes. When the joint dip angle is 60°, the length of eight main cracks is 120 mm, and ten small cracks with a length of 40 mm appear along the parallel direction of the joint. When the joint dip angle is 90°, the length of the main cracks is 120 mm, and fourteen small cracks with a length of 40 mm appear along the parallel direction of the joint.

With the continuous propagation of stress wave in coal (step 60), the bifurcation of the main cracks is more obvious. When the joint dip angle is 30°, the length of the six main cracks is 160 mm, and part of the cracks (40 mm) near the joint are blocked by the joint. Two cracks with a length of 200 mm appear at both ends of the joint, and the cracks propagation direction are parallel to the joint. When the dip angle is 60°, the length of eight main cracks is 200 mm, and two cracks with a length of 200 mm and four small cracks with a length of 80 mm appear near the two ends of the joint near the permeability enhancement holes. When the dip angle is 90°, the length of the main cracks is 240 mm, and the cracks on both sides of the joint are approximately symmetrical due to the influence of the approximately symmetrical stress wave. There are 20 cracks with the length of 80 mm on both sides of the joint.

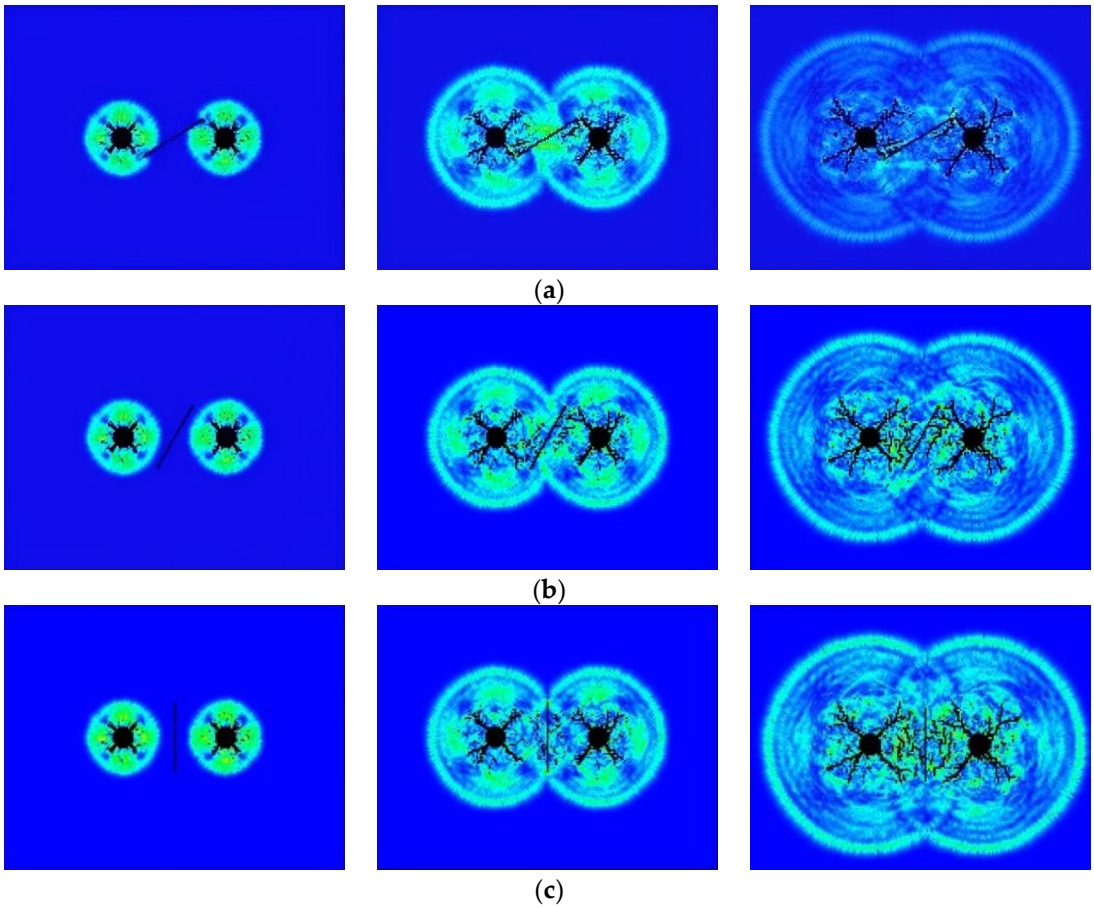

Figure 8. The cracks propagation process of high-energy gas impact permeability enhancement with different joint dip angles: (**a**) The propagation process of high-energy gas impact cracks with joint dip angle of 30°; (**b**) The propagation process of high-energy gas impact cracks with joint dip angle of 60°; (**c**) The propagation process of high-energy gas impact cracks with joint dip angle of 90° (Step 20, step 40, step 60 from left to right).

To sum up, under the action of the impact wave (step 20), the hole wall is broken. As the impact wave attenuates to stress wave, four main cracks with equal length and

symmetrical distribution appear around the wall of each hole. At this time, the joint dip angle has no effect on the crack propagation. With the propagation of stress wave in coal (step 40), the length of the main cracks increases with the increase in dip angle. Some main cracks appear a bifurcation phenomenon, and the damage and micro-damage on both sides of the main cracks increase. Cracks appear near the hole's side at both ends of the joint, and the damage degree is close. With the increase in dip angle, the damage range increases. With the propagation of shock wave in coal and the superposition of waves (step 60), the main cracks continue to extend, and the number of bifurcation cracks increase. The cracks on both sides of the joint also extend and increase, and the extension direction is approximately parallel to the joint. As the dip angle increases, the number of cracks increases and the range of extension increases, which is close to the permeability enhancement holes, forming a crack network. When the joint dip angle is 30°, the two ends of the joint are close to the permeability enhancement holes, which hinders the extension of the initial main cracks near the two ends of the joint, and the permeability enhancement effect shows an obvious zoning phenomenon. When the joint dip angles are 60° and 90°, the number of cracks is large and the cracks network is formed. With the increase in the dip angle, the cracks are more developed. Therefore, when the joint dip angle is less than 30°, the permeability enhancement effect is not ideal. When the joint dip angle is between 30° and 90°, the larger the joint dip angle is, the more cracks are generated and the better the permeability enhancement effect is.

3.2. Influence of Joint Length on Cracks Propagation Law

Due to the limitation of space, the cracks propagation process is analyzed by taking the joint dip angle of 60°as an example, as shown in Figure 9.

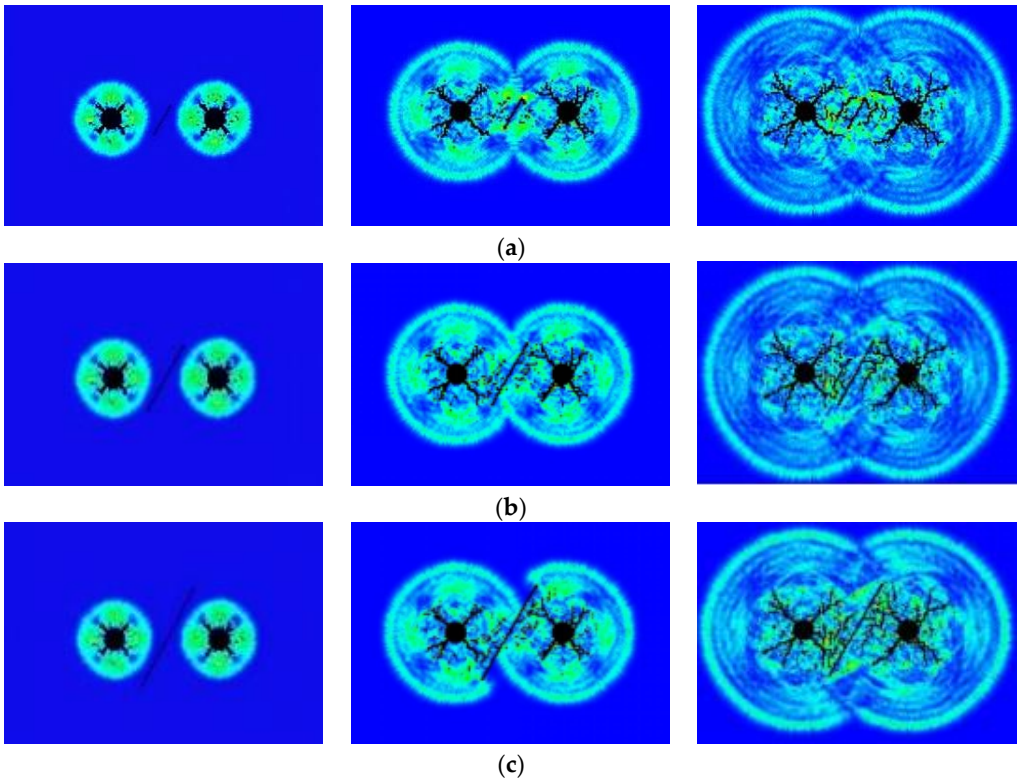

Figure 9. Cracks growth process of high-energy gas impact permeability enhancement with different joint lengths: (**a**) The cracks propagation process of high-energy gas impact permeability enhancement when the joint length is 0.2 m; (**b**) The cracks propagation process of high-energy gas impact permeability enhancement when the joint length is 0.4 m; (**c**) The cracks propagation process of high-energy gas impact permeability enhancement when the joint length is 0.6 m (Step 20, step 40, step 60 from left to right).

Under the action of shock wave, the walls of the permeability enhancement holes are broken (step 20). As the shock wave attenuates to stress wave, four uniform and symmetrical main cracks appear around the wall of each hole, and the length of the main cracks is 40 mm.

With the propagation of stress wave in coal (step 40), the two ends of the joint are approximately uniformly destroyed, the influence of the joint on the wave propagation on both sides is the same, the cracks are approximately uniformly and symmetrically distributed, and the bifurcation occurs in the main cracks around each permeability enhancement hole. When the joint length is 0.2 m, the length of eight main cracks increases to 80 mm, and six small cracks of 40 mm length appear on both sides parallel to the joint. When the joint length is 0.4 m, the eight main cracks are 120 mm, and 10 small cracks with 40 mm length appear along the parallel direction of the joint. When the joint length is 0.6 m, the length of the main cracks is 120 mm, and twenty-two small cracks of 40 mm length appear along the parallel direction of the joint.

With the continuous propagation of a stress wave (step 60) in coal, the bifurcation of the main cracks is more obvious. When the length of the joint is 0.2 m, the length of the eight main cracks is 200 mm, and there are two cracks with a length 40 mm and two cracks with length 120 mm around the joint. When the joint length is 0.4 m, eight main cracks of 200 mm length appear around the permeability enhancement holes, and two cracks of 200 mm length and four small cracks of 80 mm length appear at the two ends of the joint near the permeability enhancement holes. When the joint length is 0.6 m, eight main cracks of 200 mm length appear around the permeability enhancement holes, and two cracks of 200 mm length and six small cracks of 80 mm length appear at the two ends of the joint near the permeability enhancement holes.

In summary, the joint length has no obvious effect on the propagation of the main cracks, but has an obvious effect on the secondary cracks. With the increase in joint length, the length and number of the secondary cracks show an increasing trend, and the cracks network formed by permeability enhancement is also developed. Under the action of impact wave, the hole wall is broken. As the impact wave attenuates to stress wave, four main cracks with equivalent length and symmetrical distribution appear around the hole wall of each hole. With the propagation of the stress wave in the coal body (step 40), some main cracks result in bifurcation, and the damage on both sides of the main cracks and small damage increase. At the two ends of the joint there appear cracks near the holes side, and the damage degree is close, and with the increase in length, the damage range increases. With the propagation of shock wave in coal and the superposition of waves (step 60), the main cracks continue to extend, and the number of bifurcation cracks increase. The cracks on both sides of the joint also extend and merge, and the extension direction is approximately parallel to the joint. With the increase in the joint length, the number and length of the cracks increase, and the extension ranges are gradually close to the joint length, and the cracks network is formed among the cracks and the permeability enhancement holes. Therefore, the greater the joint length, the better the permeability enhancement effect.

3.3. Relationship between Joint Parameters and Cracks Length and Number

The final results of each test scheme are shown in Figure 10, and the number of cracks of different lengths in each scheme is counted, as shown in Figure 11.

It can be seen that with the increase in joint dip angle from 30° to 90°, when the joint length is 0.2 m, the number of cracks increases from 10 to 22 with the increase in dip angle, and when the joint length is 0.4 m, the number of cracks increases from 10 to 28 with the increase in dip angle, and when the joint length is 0.6 m, the number of cracks increases from 10 to 32 with the increase in dip angle. Therefore, the larger the joint dip angle is, the more the number of cracks is, and the longer the joint length is, the more it increases. When the joint length increases by 0.2 m, the total number of cracks increases by 4~6.

The greater the dip angle of the joint, the greater the length of the main cracks. When the joint dip angle is 30°, the main cracks length is 160 mm, when the joint dip angle is

60°, the main cracks length is 200 mm, and when the joint dip angle is 90°, the main cracks length is 240 mm. When the joint length is 0.2 m, the proportion of cracks less than 120 mm increases from 20% to 64%, when the length is 0.4 m, the proportion increases to 71%, and to 75% when the length is 0.6 m. Therefore, the larger the joint dip angle is, the larger the proportion of small cracks is, and the longer the joint length is, the more it increases. When the joint length increases by 0.2 m, the proportion of small cracks increases by about 5%.

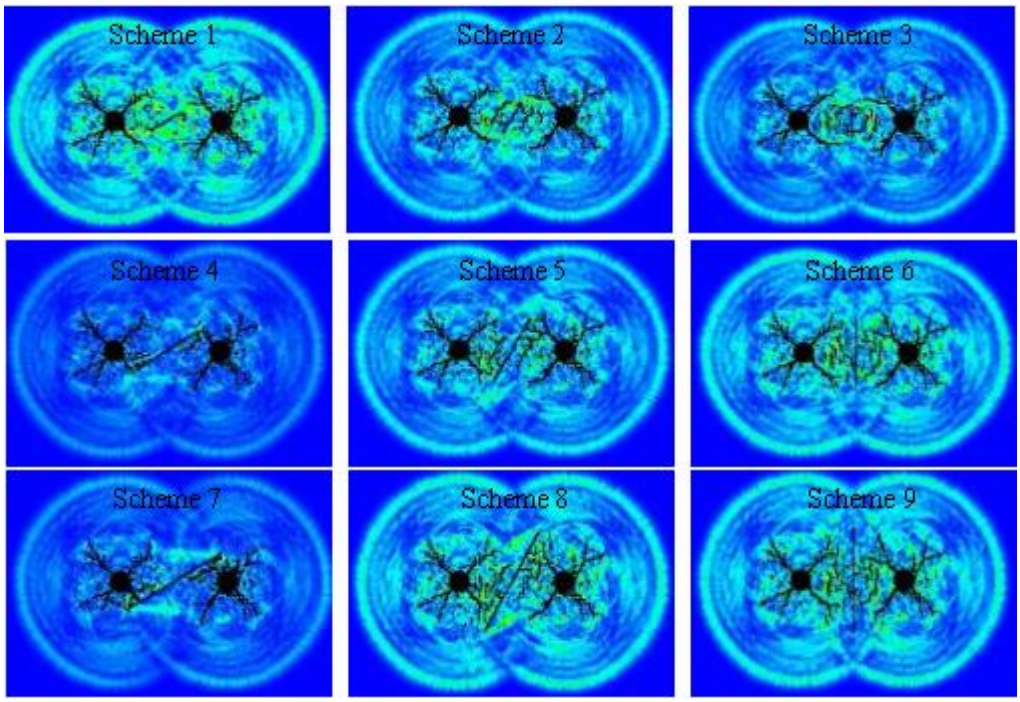

Figure 10. The cracks distribution diagram of different joint parameters.

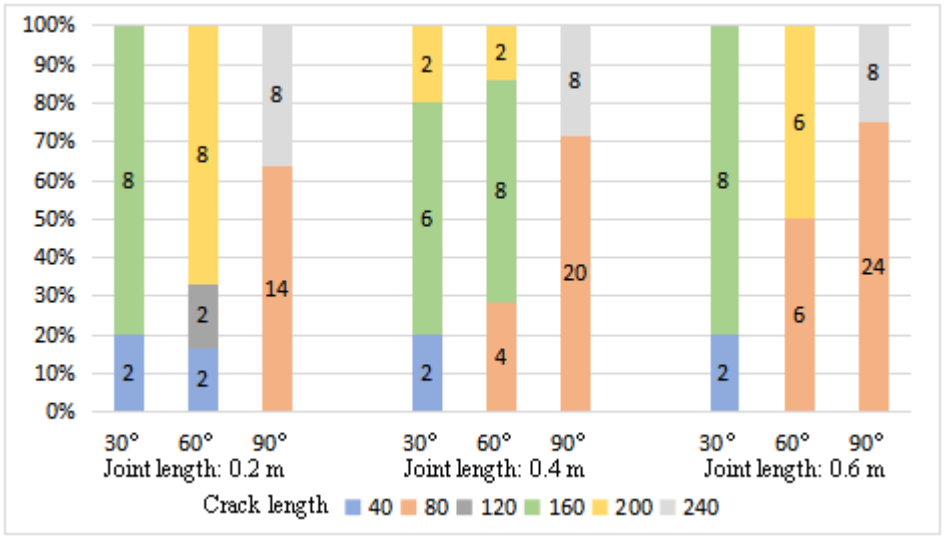

Figure 11. The proportion of cracks number of different permeability enhancement schemes.

3.4. Relationship between Joint Dip Angle, Joint Length and Cracks Permeability Enhancement Area

The statistical results of the permeability enhancement area of each scheme are shown in Tables 3 and 4. As the impact wave attenuates to the propagation of stress wave in coal, the area of cracks permeability enhancement changes greatly. In some cases, there

are a large number of cracks, but because the length of the cracks is small, the distribution of the area of the cracks' permeability enhancement area and the number of cracks is not completely consistent. The area of the cracks is related to the dip angle and length of the joint. When the joint dip angle is 30°, the joint length increases and the crack area decreases. However, when the joint dip angle is 60° and 90°, the joint length increases and the crack area increases.

Table 3. Cracks area of scheme 1 to 9 (m^2).

Scheme	1	2	3	4	5	6	7	8	9
Area	0.891	0.876	0.877	0.923	0.999	1.056	0.976	1.052	1.093

Table 4. Comparison table of two factors affecting crack area.

Scheme	Dip Angle Range	Length Range	Influence Factors of Dip Angle	Influence Factors of Length
1	0.01	0.066	A	B
2	0.005	0.1	B	A
3	0.004	0.113	B	A
4	0.007	0.034	B	A
5	0.006	0.023	B	A
6	0.063	0.086	B	A
7	0.011	0.099	B	A
8	0.015	0.076	B	A
9	0.026	0.123	B	A

Note: The range method is used to compare the influence of the two factors on the area, and the influence factor A > B.

The influence of joint length on cracks area and cracks propagation is greater than that of joint dip angle. By comparing the number of cracks with the same method, it can be concluded that the influence of joint length is greater than that of joint dip angle. Therefore, in the impact permeability enhancement of high-energy gas, the first consideration is the joint length, and the second is the joint dip angle. At the same time, according to the statistical results of Table 5, all the test data points of joint dip angle, length and permeability enhancement damage area are fitted by the least square method, and the surface fitting results are solved at one time. The least square method is used to fit the joint parameters and the permeability enhancement crack area surface fitting results as shown in Figure 12, the Adjusted R-square reaches 92.18%.

Table 5. Statistical results of cracks area (m^2) with different joint parameters.

Joint Length/m \ Joint Dip Angle/°	30	60	90
0.2	0.891	0.923	0.976
0.4	0.876	0.999	1.052

Surface equation: $S = 1.04 - 1.279 \times 10^{-2}x - 2.731 \times 10^{-1}y + 2.598 \times 10^{-4}x^2 + 1.63 \times 10^{-2}xy - 1.33 \times 10^{-2}y^2 + 1.518 \times 10^{-6}x^3 + 8.902 \times 10^{-5}x^2y - 2.122 \times 10^{-3}xy^2$

In the formula:

X—joint dip angle (°),

Y—joint length (m),

S—permeability enhancement crack area (m^2).

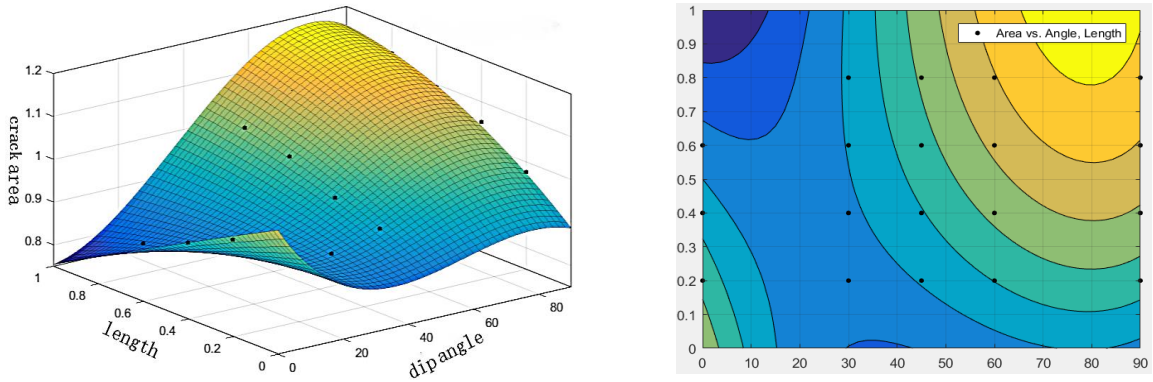

(**a**) (**b**)

Figure 12. The least square method fitting results of different joint parameters with the cracks area (m^2): (**a**) Fitting surface of cracks area with different joint parameters; (**b**) The plane projection of cracks area with different joint parameters.

4. Conclusions

The main results are as follows:

(1) In the process of impact permeability enhancement of high-energy gas, the wave gradually attenuates to shock wave, stress wave and seismic wave, forming three different regions: crushing zone, crack zone and elastic-plastic zone.

(2) The influence of joint orientation on high-energy gas seepage cannot be ignored, and the simulation results show the influence of joint orientation. Under the action of the stress wave, when the joint is close to the permeability enhancement holes, the main cracks will be suppressed, but the main cracks far away from the joint will not be affected. The distribution of the secondary cracks is also related to the orientation of the joint. The cracks first appear on the side of the joint near the permeability enhancement holes, and then with the continuous propagation of the stress wave, the cracks continue to propagate in the direction parallel to the joint, while the secondary cracks far away from the joint bifurcate on the basis of the main cracks.

(3) The walls of the permeability enhancement holes are broken under the action of the impact wave. As the impact wave attenuates to stress wave, four main cracks of equal length and uniform symmetrical distribution appear around the hole wall of each hole. The cracks' development and permeability enhancement effect are related to the dip angle and length of the joint.

(4) At the initial stage of impact permeability enhancement of high-energy gas, the effect of joint dip angle on cracks propagation is not obvious, and with the propagation of stress wave, the length of the main cracks increases with the increase in dip angle. The extension direction of the secondary crack is approximately parallel to the joint, and with the increase in the dip angle, the more the number of the secondary cracks is, the larger the extension range is, and the closer it is to the permeability enhancement holes, the cracks network is formed.

(5) When the dip angle of the joint is 30°, the permeability enhancement effect results in an obvious zoning phenomenon. When the dip angle of the joint is 60° and 90°, the number of cracks is more, and the cracks network is formed, and with the increase in the dip angle, the more the cracks develop and the better the permeability enhancement effect.

(6) The effect of joint length on the propagation of the main cracks is not obvious, but on the secondary cracks it is obvious. With the increase in joint length, the length and number of secondary cracks increase, and the cracks network formed by permeability enhancement is also developed. The longer the joint length is, the better the permeability enhancement effect is. The influence of joint length on cracks' area and cracks' number is greater than that of joint dip angle.

(7) The larger the dip angle of the joint is, the higher the number of cracks, and the longer the joint length is, the more it increases. When the joint length increases by 0.2 m, the total number of cracks increases by 4~6. The larger the joint dip angle is, the larger the proportion of small cracks is, and the longer the joint length is, the more it increases. When the joint length increases by 0.2 m, the number of small cracks increases by about 5%. The mathematical relationship between joint dip angle, joint length and cracks area is quantified and established, and the quantitative representation of cracks and joint parameters is realized.

Author Contributions: Conceptualization, D.D.; methodology, X.F.; software, W.L.; validation, H.Z., X.C. (Xiaoyu Chen) and S.G.; formal analysis, X.C. (Xi Chen); investigation, X.W.; data curation, A.W.; writing—original draft preparation, X.C. (Xi Chen); writing—review and editing, D.D.; visualization, X.F.; supervision, W.L.; project administration, D.D.; funding acquisition, D.D. and X.F. All authors have read and agreed to the published version of the manuscript.

Funding: This research was funded by the National Natural Science Foundation of China (grant No. 52274134, No. 51604184 and No. 51304143).

Institutional Review Board Statement: Not applicable.

Informed Consent Statement: Not applicable.

Data Availability Statement: The data used to support the findings of this study are available from the corresponding author upon reasonable request.

Conflicts of Interest: All authors declare no competing interest in this study.

References

1. Kang, X.T.; Jiang, M.Q.; Huang, G.; Wu, J.N.; Tang, M.; Wang, Z.Y. Application research on fracture propagation law of combined hydraulic pressure in multiple coal seams. *J. Min. Saf. Eng.* **2021**, *38*, 602–608. [CrossRef]
2. Sun, S.Q.; Zhang, Q.; Yan, Z.M.; Zhang, J.; Wang, Y.W.; Zheng, K.G. Practice of permeability enhancement through overall hydraulic fracturing of long hole in outburst-prone soft crushed coal seam with low permeability. *J. China Coal. Soc.* **2017**, *42*, 2337–2344. [CrossRef]
3. Ma, S.Y. Research on permeability increasing technology of low permeability combined rock coal seam. *IOP Conf. Ser. Earth Environ. Sci.* **2021**, *804*, 022055. [CrossRef]
4. Ni, G.H.; Xie, H.C.; Li, Z.; Zhuansun, L.X.; Niu, Y.Y. Improving the permeability of coal seam with pulsating hydraulic fracturing technique: A case study in Changping coal mine, China. *Process. Saf. Environ. Prot.* **2018**, *117*, 565–572. [CrossRef]
5. Chen, J.H.; Liu, L.; Zeng, B.Q.; Tao, K.M.; Zhang, C.; Zhao, H.B.; Li, D.Q.; Zhang, J.W. A constitutive model to reveal the anchorage mechanism of fully bonded bolts. *Rock Mech. Rock Eng.* **2022**, *56*, 3. [CrossRef]
6. Zheng, K.G. Permeability improving technology by sectional hydraulic fracturing for comb-like long drilling in floor of crushed and soft coal seam with low permeability. *J. Min. Saf. Eng.* **2020**, *37*, 272–281. [CrossRef]
7. Li, D.; Lu, Y.Y.; Rong, Y.; Zhou, D.P.; Zhang, S.B.; Zhang, C.K. Rapid uncovering seam technologies for large cross-section gas tunnel excavated through coal seams using directional hydraulic fracturing. *Rock. Soil. Mech.* **2019**, *40*, 363–369+378. [CrossRef]
8. Liu, S.L.; Zhu, C.J.; Lin, B.Q.; Liu, T. The effect of spatial distribution mode of hydraulic slotting on pressure relief and permeability enhancement of the coal seam. *J. Min. Saf. Eng.* **2020**, *37*, 983–990. [CrossRef]
9. Cao, Z.Y.; Wang, E.Y.; He, X.Q.; Wang, H.; Liu, Q.L.; Zhang, G.H.; Luo, F.; Wang, C.; Xu, Y.L. Effect evaluation of pressure relief and gas drainage of hydraulic punching in short-distance coal seam group with the risk of outburst. *J. Min. Saf. Eng.* **2021**, *38*, 634–642. [CrossRef]
10. Wu, B.; Li, H.L.; Meng, G.W.; Xu, S.X.; Zhang, J.L.; Cui, Y.Z. Numerical Analysis and Application of Elliptical Bipolar Linear Energy-gathering Hydraulic Control Blasting Based on SPH-FEM. *J. Railw. Eng. Soc.* **2022**, *39*, 87–93. [CrossRef]
11. Guo, D.Y.; Zhang, C.; Li, K.; Zhu, T.G. Mechanism of millisecond-delay detonation on coal cracking under deep-hole cumulative blasting in soft and low permeability coal seam. *J. China. Coal. Soc.* **2021**, *46*, 2583–2592. [CrossRef]
12. Xu, Y.P.; Wang, L.G.; Bhattacharyya, S.; Peng, X.S.; Chen, X.J. Improving safety by further increasing the permeability of coal seams using air cannons after hydraulic punching. *Arabian J. Geosci.* **2021**, *14*, 2126. [CrossRef]
13. Huang, C.G.; He, J.F.; Zhao, Z.Q. Field Tests on Permeability Enhancement Technology in Crushed and Soft Coal Seam. *IOP Conf. Ser. Earth Environ. Sci.* **2019**, *300*, 022015. [CrossRef]
14. Zhang, D.M.; Bai, X.; Yin, G.Z.; Rao, Z.; He, Q.B. Research and application on technology of increased permeability by liquid CO_2 phase change directional jet fracturing in low-permeability coal seam. *J. China Coal. Soc.* **2018**, *43*, 1938–1950. [CrossRef]
15. Bai, Y.; Sun, L.; Wei, C.H.; Li, H.Z. A Coupled Gas Flow-Mechanical Damage Model and Its Numerical Simulations on High Energy Gas Fracturing. *Geofluids* **2020**, *2020*, 3070371. [CrossRef]

16. Wu, F.P.; Wei, X.M.; Chen, Z.X.; Rahman, S.S.; Pu, C.S.; Li, X.J.; Zhang, Y.Y. Numerical simulation and parametric analysis for designing High Energy Gas Fracturing. *J. Nat. Gas. Sci. Eng.* **2018**, *53*, 218–236. [CrossRef]
17. Chen, J.H.; Zeng, B.Q.; Liu, L.; Tao, K.M.; Zhao, C.; Zhang, J.W.; Li, D.Q. Investigating the anchorage performance of full-groutedanchor bolts with a modified numerical simulation method. *Eng. Failure Anal.* **2020**, *141*, 106640. [CrossRef]
18. Guo, D.Y.; Zhao, J.C.; Zhu, T.G.; Zhang, C. Crack propagation and coalescence mechanism of double-hole cumulative blasting in coal seam. *Chin. J. Eng.* **2020**, *42*, 1613–1623. [CrossRef]
19. Guo, D.Y.; Zhang, C.; Zhu, T.G.; Li, G.T. Effect of detonating position of deep-hole cumulative blasting on coal seam cracking and permeability enhancement. *J. China Coal. Soc.* **2021**, *46*, 302–311. [CrossRef]
20. Fan, S.X.; Wen, H.; Cheng, X.J.; Zhang, C.R.; Wei, G.M.; Zhai, X.W.; Chen, J.; Zhang, D.; Liu, M.Y. Research and application of a complete set equipment of permeability enhancementes induced by high-pressure L-CO_2 fracturing. *J. China Coal. Soc.* **2020**, *45*, 801–812. [CrossRef]
21. Song, Y.Q.; Li, X.S.; Guo, D.Y. Numerical simulation of multi-hole and same delay time of cumulative blasting in coal seam and its application. *J. China Coal. Soc.* **2018**, *43*, 469–474. [CrossRef]
22. Ming, X.T.; Liu, D.Y. Numerical Simulation Research on Downhole High Energy Gas Fracturing Design. *J. Ordnance Equip. Eng.* **2021**, *42*, 158–162. [CrossRef]
23. Chen, H.B.; Ma, Z.Q.; Ai, S.J.; Luo, M.Z.; Yang, L.; He, Z.L. Research & Application of Perforating High Energy Gas Fracturing Technology. *Drill. Prod. Technol.* **2020**, *43*, 67–69. [CrossRef]
24. Ma, T.H.; Cui, C.S.; Xiao, W.C. Experimental study on the performance test system of high energy gas fracturing apparatus in coal-bed methane extraction. *J. China Coal. Soc.* **2014**, *39*, 1857–1861. [CrossRef]
25. Li, H.W.; Liu, J.; Gao, X.C.; Wang, L.G.; Sun, S.Y.; Zhu, Z.J. Effect of cold loading by liquid nitrogen on damage of coal samples with varied joint angles and water saturation levels. *J. Min. Saf. Eng.* **2022**, *39*, 413–420. [CrossRef]
26. Mu, H.W.; He, X.Q.; Song, D.Z.; Li, Z.L.; Qiu, L.M.; Su, D.F.; Yin, S. Response characteristics and influence mechanism of uniaxial compression mechanics and AE of coal with different joint angles. *J. China Coal. Soc.* **2020**, *45*, 1726–1732. [CrossRef]
27. Zhao, J.J.; Zhang, Y.; Ranjith, P.G. Numerical modelling of blast-induced fractures in coal masses under high in-situ stresses. *Eng. Fract. Mech.* **2020**, *225*, 106749. [CrossRef]